STRUCTURAL AND OPTICAL PROPERTIES OF Cr^{+3}-SUBSTITUTED Co-FERRITE SYNTHESIS BY COPRECIPITATION METHOD

M. AZIM[a], M. A. CHAUDHRY[a], N. AMIN[b], M. I. ARSHAD[b], M. U. ISLAM[c], S. NOSHEEN[d], M. AHMAD[e], H. ANWAR[f], M. WASEEM[a] ,G. MUSTAFA[c*]

[a]*Department of Physics, University of Sargodha Lyallpur Campus Faisalabad - 38000, Pakistan*

[b]*Department of Physics, G.C University Faisalabad, 38000, Pakistan*

[c]*Department of Physics, Bahauddin Zakariya University Multan 60800, Pakistan*

[d]*Department of Physics, UET Lahore (Faisalabad Campus), Pakistan.*

[e]*Department of Physics, COMSATS Institute of Information Technology, Lahore-54000, Pakistan*

[f]*Department of Physics, University of Agriculture Faisalabad 38040, Pakistan*

A series of nanocrystalline Cr-substituted $CoCr_xFe_{2-x}O_4$ ferrite powder ($x = 0.0 \leq x \leq 0.10$ with an interval of 0.02) has been synthesized by co-precipitation technique, the powder sintered at 900^0C for 6h. X-ray diffraction (XRD) and Fourier Transform Infrared Techniques (FTIR) were employed for the confirmation of the formation of spinel cubic structure. The X-ray diffraction pattern revealed that secondary phase with increasing Cr^{+3} contents $x>0.04$. Moreover, the average crystallite size of the synthesized samples was found to be ranging from 70.4- 31.5 nm while lattice parameters decrease with increasing chromium contents. Fourier transform infrared techniques data shows the formation of two frequency bands tetrahedral and octahedral bands which are the basic characteristics of cubic spinel ferrites that corresponds to the metal oxide. Morphology of the spinel ferrites powder was analyzed by scanning electron microscope (SEM) and atomic force microscopy (AFM) technique. The observed results are explained on the basis of crystal size and elemental composition which were verified by energy dispersive X-ray spectroscopy (EDX). Furthermore, the effect of Cr^{+3} on the structural and optical properties was studied by UV-visible spectra. The band gap energy for the sample having $x = 0.10$ lies from 2.5 to 4.5 eV, while the Photoluminescence (PL) spectra have the maximum peak at about 3500 nm with an energy of 0.356 eV.

(Received June 6, 2016; Accepted September 3, 2016)

Keywords: Spinel ferrites; co-precipitation; X-ray diffraction;Band gap Optical Properties.

1. Introduction

Ferrites have been the subject of researchers interest because of their importance in many technological applications ranging from microwave to radio frequencies **[1]**. The development of innovative materials is the essential part of research **[2]**. An important class of semiconductors ferrites, oxides of different transition metals has remarkable applications in magnetic storage media, transformer core, ceramic coatings for solar cells and optoelectronic devices **[3-5].** Many researchers have tailored ferrites with the addition of trivalent ions including Al^{3+} and Cr^{3+} in cobalt ferrite due to high annealing temperature and the cation distribution mechanism of Al,Cr cobalt ferrite. The ferric ions are distributed among octahedral B site and tetrahedral A site lattice position in magnetically diluted ferrites. The introduction of nonmagnetic ions on octahedral B sites will cause a decrease in the crystallite size of the synthesis material. An increase in Cr^{3+} concentration has been reported to increase the normalized susceptibility and decreases the Neel temperature **[7-9]**. Furthermore, the addition of chromium in ferrites was reported to cause the variations in band gap energy **[10-12]**.The grain size distributions of metallic ions among the

*Corresponding author: ghulammustafabzu@gmail.com

crystallographic crystal lattice sites have a remarkable influence on the properties of the ferrites.To attain these grain sizes several methods are used to prepare nano-materials **[13]**. Katalin et al **[14]** has presented that the variations in the properties of ferrites depend on the preparation method, sintering temperature, sintering time, the type and the amount of the additive. In this method, the desired nano particles in ferrites samples are synthesized by controlling the rate of reaction. The ferrites are also synthesized with different techniques, sol-gel auto-combustion method **[16]**, micro emulsion **[17]**, microwave plasma **[18]**, mechanical milling **[19]**, and co-precipitation **[20]**.The co-precipitation method has been the attractions of many scientists for the preparation of nano-sized ferrite because of various advantages such as, good stoichiometric control, production of ultrafine particles with a narrow size distribution in a relatively short processing time and at a very low temperature. The aim of present work is to investigate the effect of chromium substitution on the structural and optical properties of cobalt ferrite $CoCr_xFe_{2-x}O_4$ synthesized via co-precipitation method and sintered at 900 ^oC for 6 h.

2. Materials and Methods

2.1. Samples preparation and Equipments

The chemical regents including $Co(NO_3)_2.6H_2O$,$Cr(NO_3)_2.6H_2O$ and $Fe(NO_3)_3.9H_2O$ (Aldrich, 99%) were used to prepare the samples with formula $CoCr_xFe_{2-x}O_4$(where $0.0 \leq x \leq 0.10$) by co-precipitation method. These chemicals were weighed with desired stoichiometric proportion and dissolved in deionized water for 30 min using an ultrasonic bath. In heating process, the solution was stirred continuously with a magnetic stirrer. After this sodium hydro oxide 2.5 M was added drop wise until the pH of the solution attained a value of 10-11. Intermediate precipitates were observed in the solution which further stirred for 1 hr to maintain the homogeneity. The resulting precipitates along with solution were digested on water bath at 85 $^{\circ}C$ for 1hr under the ambient atmosphere and then the precipitates were filtered by a filter paper (No.41) with the help of a suction flask operating on the vacuum pump. Finally, these precipitates were washed with distilled water to remove impurities. The obtained precipitates were dried at 110 $^{\circ}C$ for 12 h in an oven. These dried precipitates were mixed homogeneously in an agate mortar and pestle for 30 min. The powders were sintered at 900 $^{\circ}C$ for 6 h in a programmable furnace and slowly cooled down at room temperature to yield the final product. The X-ray diffraction (XRD) patterns were obtained at room temperature by powder samples in an Xpert Pro PANalytical diffract meter with Cu-Kα radiation (λ = 1.5405 Å) at 40 kV and 30 mA. Intensity data were collected by step counting method (with a scanning speed 0.02° /s) in the 2θ range from 20-70°.In addition, surface morphology and microstructure of the samples were studied by JSM-6490 JEOL scanning electron microscope (SEM). The elemental composition was determined by energy dispersive peak of the representative sample using energy dispersive X-ray spectroscopy (EDXS, Model JFC-1500 JEOL).FT-IR spectrum was recorded using Perkin-Elmer infrared spectrometer Model C-783 in the range 450–800 cm^{-1}. Morphological studies were done using Atomic Force Microscopy (AFM), Digital instruments Nano scope-E, with Si_3N_4 100 nm cantilever, 0.58 N/m force constant measurements in contact mode. UV–visible absorption spectra were recorded using a UV-vis-NIR spectrophotometer (Perkin Elmer Lambda 9) at room temperature and Photoluminescence (PL) spectra.

2.2 Calculations

The structural parameters such as lattice constant, unit cell volume; crystallite size and X-ray density were calculated from X-ray diffraction data using the following formulae [21-23]. The lattice constant values have been computed using the d-spacing values and the respective Miller indices (hkl) from the classical formula as given below.

$$a = \frac{\lambda}{2Sin\theta}\sqrt{h^2 + k^2 + l^2} \quad (1)$$

The spinel cubic unit cell volume was calculated

$$V_{cell} = a^3 \quad (2)$$

The crystallite size (D) nm was determined by using the Scherer's equations.

$$D = \frac{k\lambda}{B_{(hkl)}\cos\theta} \quad (3)$$

Where k is the shape coefficient (value between 0.9 and 1.0), λ is the X-ray wavelength, B is the full width at half maximum (FWHM) of each Phase and θ is the Bragg's diffraction angle. The X-ray density was determined according to the relation:

$$\rho_{X-ray} = \frac{Z\,M}{N_A\,V} \quad (4)$$

Where, V is the unit cell volume, Z represents 8 molecules per unit cell of the spinel structure, N_A is the Avogadro's number and M is the molecular weight of the sample.

3. Results and Discussions

3.1. Crystal Structure Analysis

Fig.1 shows the X-ray diffraction patterns of $CoCr_xFe_{2-x}O_4$ (where $0.0 \leq x \leq 0.10$ with interval 0.02) ferrite system synthesized by co-precipitation technique and sintered at 900 °C for 6 h.

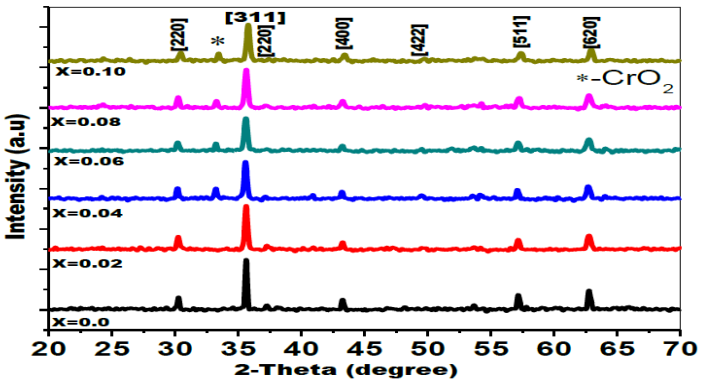

Fig.1. X-ray diffraction patterns of Cr-substituted Co- ferrites (0 < x < 0.10).

All peaks were indexed and verified from computer software library and found that X-ray diffraction patterns were belongs to Fd_3m space group. An additional line has been observed at about 33° which represents a secondary phase that may be appeared due to exceeding the limit of Cr solubility after x= 0.04. Moreover, these diffraction peaks corresponding to the planes (220), (311), (222), (400), (422), (511/333) and (440) confirmed the synthesis of spinel ferrite structure. The physical properties of X-ray diffraction parameters were calculated using Eq.1-4 and listed in

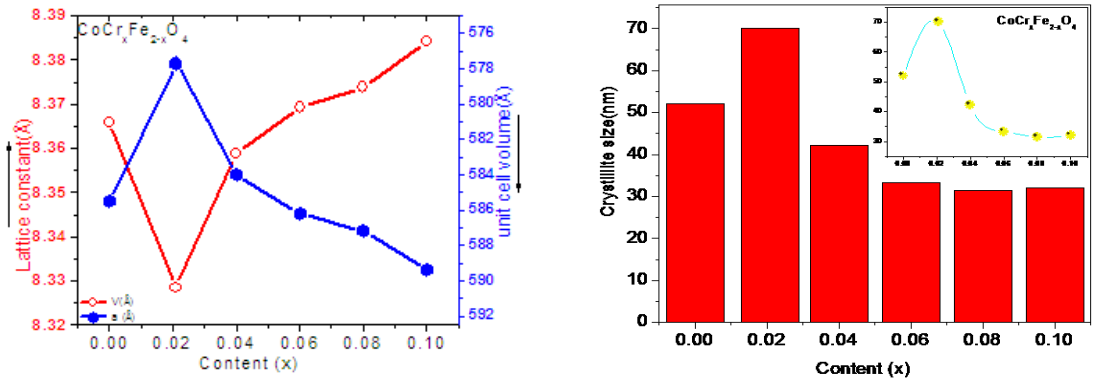

a) b)

Fig.2. a) Effect of lattice parameters and unit cell volume vsC r-content
b) crystallite size vs Cr-substituted Co- ferrites (0 < x < 0.10).

Table 1.The value of lattice constant and unit cell volume for all the samples are found to increase with the increase of Cr^{3+} contents which may be due to a difference in their ionic radii while for the pure cobalt ferrite sample have the values of lattice constant 'a' is 8.3659 Å. The comparative graph of the lattice constant and unit cell volume depicted in the Fig.2 which exhibits similar increasing trend corresponding with Cr^{3+} content. Furthermore, the crystallite size are calculated by the Eq.3 using high intensity peak (311).The crystallite size is found as 52.2 nm for pure (x = 0.00) while the crystallite size decreases with increasing Cr^{3+}substitution as the substituent ions inhibiting the grain growth. Besides, it is observed that the crystallite size lies in the ranges 31.5-70.4 nm (listed in Table 1). At x = 0.00 and 0.02 samples have below crystallite sizes ≤ 50 nm which are suitable for signal to noise ratio in the high density recording media[24].The X-ray density of all the samples was calculated by the Eq.4.(listed in Table 1). The effect of chromium ions on the X-ray density reveals that the synthesized material have increasing trend with increases the substituent ions which is due to the molar mass difference as compared to Cobalt (58.93 amu),Chromium (52.00 amu) and iron (55.85amu).

Table 1.Lattice constant, volume of the unit cell, Crystallite size (nm), X-ray density (d_x) of Cr substituted Co-ferrites annealed at 900°C for 6h

Parameters/Contents (x)	**x= 0.00**	**x= 0.02**	**x= 0.04**	**x= 0.06**	**x= 0.08**	**x= 0.10**
Lattice constant, a (Å)	**8.3659**	**8.3285**	**8.3587**	**8.3692**	**8.3738**	**8.3842**
Volume of the unit cell ($Å^3$)	**585.52**	**577.70**	**584.00**	**586.21**	**587.18**	**589.37**
Crystallite size $<D>_{MCD}$ (nm)	**52.2**	**70.4**	**42.2**	**33.3**	**31.5**	**32**
$d_x(g/cm^3)$	**5.31**	**5.29**	**5.30**	**5.33**	**5.33**	**5.39**

3.2 FTIR spectra studies

FTIR spectra of the representative samples recorded in the wave number range 450–800 cm^{-1} is shown in Fig.3. The presence of two absorption bands below 1000 cm^{-1} is a common feature observed in all ferrites [25].

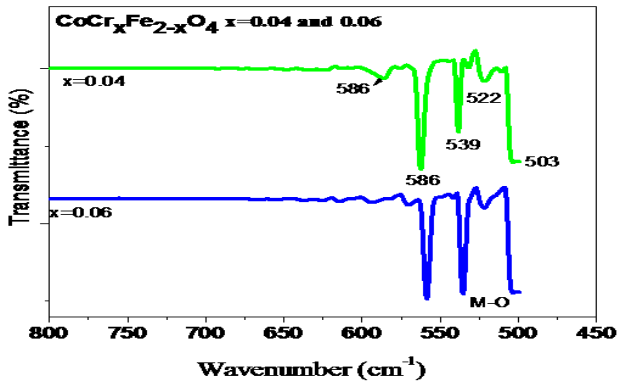

Fig.3. FTIR spectra of the Cr-substituted Co-ferrites (x=0.04 and 0.06)

Moreover, in this investigation polycrystalline cubic spinel ferrites absorption bands of metal oxides are attributed to the intrinsic vibrations of the tetrahedral and octahedral group complexes samples at x = 0.04 and 0.06. The change in the peak intensity of the spectra has been noticed with increasing Cr^{3+} contents. It is well known that the intensity ratio is a function of the change of dipole moment with the inter-nuclear distance [21] that represents the contribution of the ionic bond Fe–O in the lattice. Hence the observed increase in the peak intensity is attributed to the perturbation occurring in Fe–O bonds by the substitution of chromium ions for x = 0.04 and 0.06 and such similar results have been reported [26].

3.3 Morphology and Elemental analysis

Fig.4 shows the scanning electron microscope micrographs of representative samples which exhibit the homogeneous grain size distribution in the range of nanometer region and grains seem to be spherical in shape. Micrographs revealed few voids and pores which can be seen very clearly, thus the synthesized material is a porous nature ferrites material. Moreover, grains have shown crystalline structure of spinel ferrite which was justified by XRD studies. Furthermore, it is observed that the investigated ferrite samples have agglomerates which may be attributed to sintering process as a result of chemical reaction. Magnetic forces or weak Vander Waals bonds might be responsible to hold these agglomerates together [27].

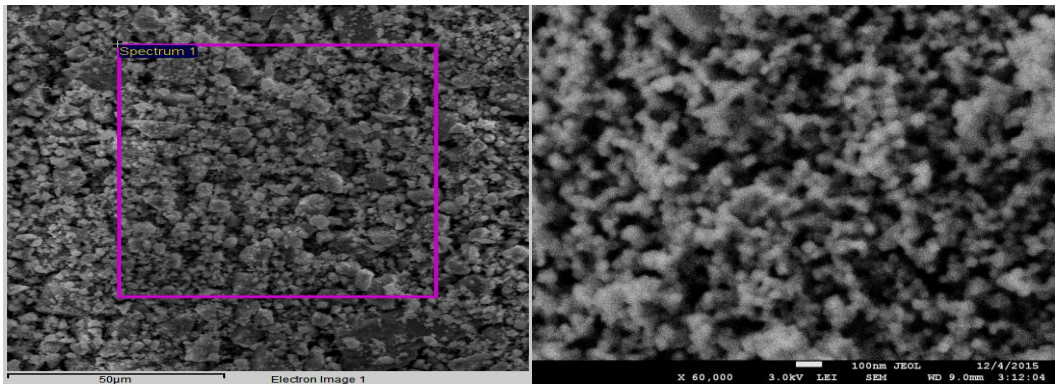

Fig. 4 SEM Micrographs for Cr-substituted Co-ferrites at x=0.02 and 0.04

Fig. 5 shows the energy dispersive X-ray spectra of the representative composition of the investigated sample. The analysis of these spectra indicates that mixed oxides have fully undergone the chemical reaction to form the required oxide materials. The results confirmed that most of the undesired precursor materials like nitrates ions have been completely removed from the final product. The spectra exhibits the different orbital states of Co,Cr, Fe and O which suggest that the observed ratio of all the atoms is close to the reported values. Fig. 6 shows the atomic force microscopy (AFM) images of one of the selected sample which gives the complimentary information about the surface morphology, shape and size of the particles synthesized by co-precipitate method. The results confirmed that the sample morphology and cubic spinel structure lies in the nano size particle which observed by AFM, was also in consistent with the results of SEM and XRD analysis.

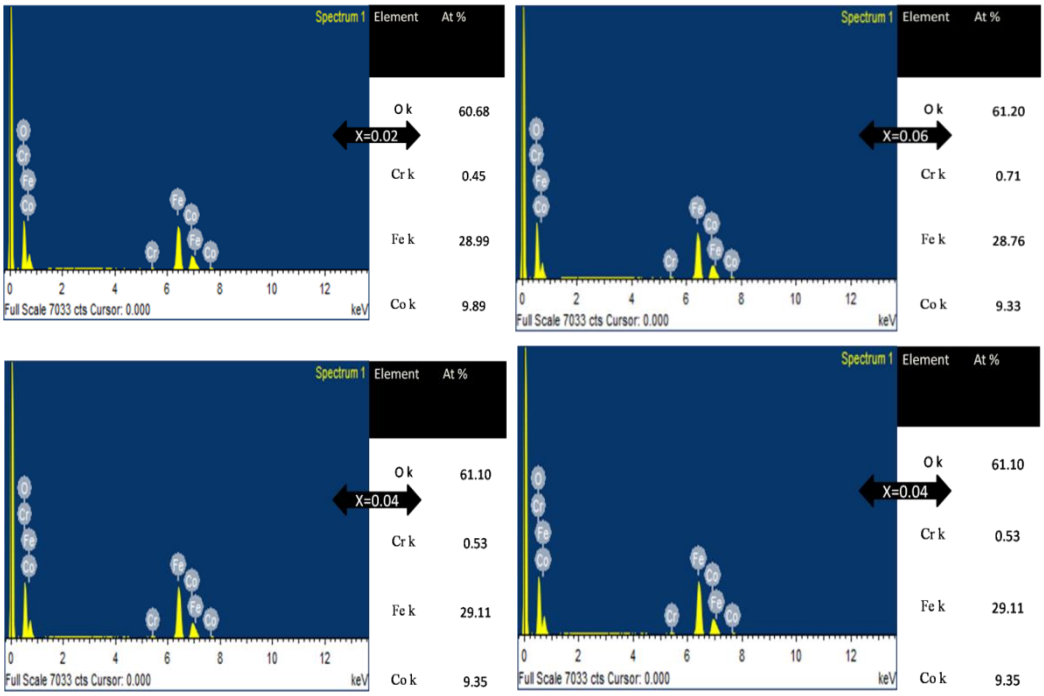

Fig. 5 EDX Spectrum for Cr-substituted Co-ferrites at x= 0.02, 0.04, 0.06 and 0.10.

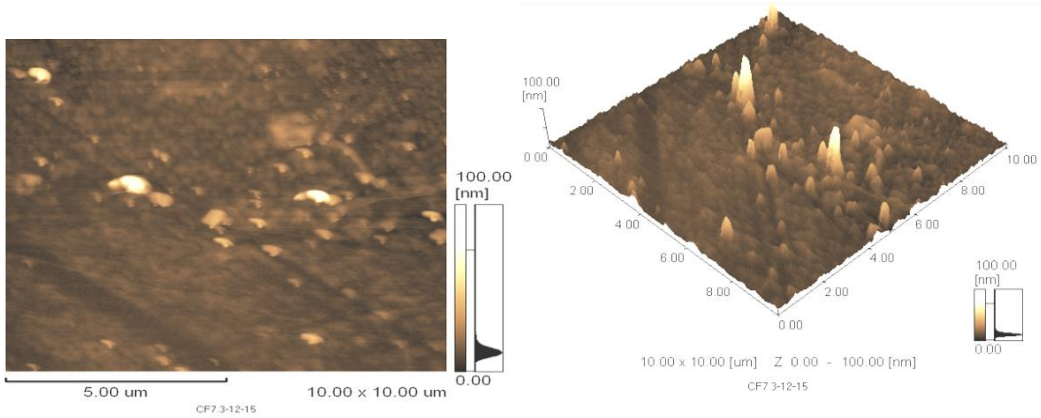

Fig.6 AFM images of the Cr-substituted Co-ferrites x = 0.04

3.4 Optical Properties

Study of optical properties at room-temperature such as absorption, reflection, transmission of light and band gap energy is of a great importance in optoelectronics applications. Fig.7 (a & b) shows that the reflectance (%R), transmittance (%T) variation for chromium substituted cobalt ferrites as the function of wavelength in the UV-visible region (200-1100 nm).

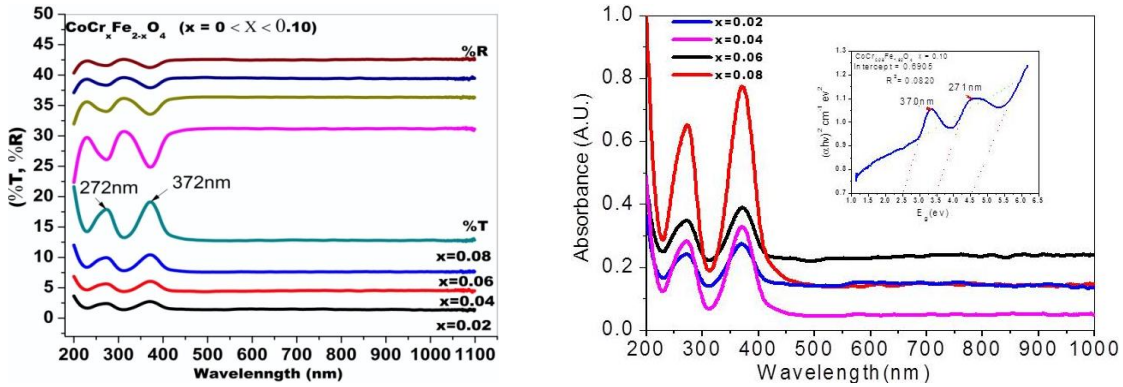

a) b)

Fig.7 Spectral transmittance T and reflectance R of the Cr-substituted Co-ferrites (x=0.02, 0.04, 0.06 and 0.08) sintered at 900 °C for 6 h (b) plot $(\alpha hv)^{1/2}$ versus $E_g(ev)$

The sharp peak at 272 nm and 372 nm in the UV–visible spectra indicates that the colloids are well dispersed. The plot clearly presents the inverse relation of (%T) as compare to (%R) which can be observed from the Fig.7 it shows the (%T) behavior enhances as the contents of chromium are increased from x = 0.02 to x = 0.08 and its wavelength lies most prominently in UV region wavelength 200-380 nm approximately. At x = 0.08 the (%R) is ~ 30% while x = 0.02 (%T) is ~ 2.5% which shifts to ~ 15-20 % for x = 0.08.Chandan et al [28] has been reported similar behavior of the absorption bands. The optical band gap for representive sample have shown in the inset Fig.7 and calculated by Tauc relation:

$$\alpha hv = A(hv - E_g)^n \tag{5}$$

Here E_g is optical band gap, hv is photon energy, A is constant that depends on the transition probability, α is absorption coefficient and the value of n is 0.5 for the allowed direct band and 3/2 for forbidden direct energy gap for ferrites material [29-30]. The value of absorption coefficient α can be calculated using this relation $\alpha = {}^{4\pi k}/_{\lambda}$ where k is absorbance (absorption index) and is the wavelength (nm).The value of the optical band gap energy (E_g) of the prepared sample for x = 0.08 is calculated by plotting Tauc's graphs between $(\alpha hv)^2$ versus (hv) photon energy as shown in Fig.7. The intercept of the graph linear region on energy axis at $(\alpha hv)^2$ equal to zero gives the band gapenergy. The observed band gap energy values are found to be (2.5, 3.5 and 4.5eV) in the product material, such kinds of behavior may be due to lattice defects, displacement of atoms and line defects resulting from grain boundary diffusion. Moreover, it is observed that the energy band gap increases whenever the particle size decreases. This can be explained on the basis of Bras effective mass model [31-32] according to which the measured band gap, *Eg* can be expressed as a function of particle size as:

$$E_g^{nano} \cong E_g^{bulk} \frac{h^2}{8m_0 r^2}\left(\frac{1}{m_e} + \frac{1}{m_h}\right) - \frac{1.8e^2}{4\pi\mathcal{E}\mathcal{E}_0 r} \tag{6}$$

Where E_g bulk is the bulk energy gap, r is the particle size, m_e is the effective mass of electrons, m_h is the effective mass of holes, ε is the relative permittivity, ε_o is the permittivity of free space, h is the planck's constant, and e is the charge on electron.

3.5. Photoluminescence Spectra

Photoluminescence behavior of spinel ferrites nanoparticles yields information on the energies and dynamics of photo generated charge carriers as well as on the nature of the emitting states. Electron from ferrite sample lies in the conduction band, excitonic states and trap states [33-37].

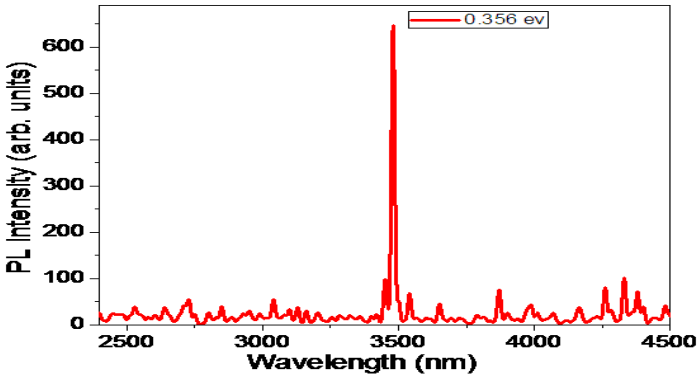

Fig.8. Shows the Photoluminescence (PL) spectra of the represented sample at the room temperature.

It is well known that emission and efficiency are very sensitive to nature of nanoparticles surface, due to the presence of gap surface states arising from surface non-stoichiometry and unsaturated bonds. Surface trap states allow non-radioactive recombination and enhance luminescence efficiency. However, in this case when the sample was annealed at 900 $^{\circ}$C, broad band emissions spectra are carried out at 3500 nm appeared in the fluorescence spectrum, (Fig. 8) shows the spectra which has energy of 0.356 eV. Moreover, photoluminescence (PL) peak is attributed to the recombination of charge carriers in deep traps of surface localized states and lattice defects [38-41]. Therefore such defects are responsible for the luminescent properties of the synthesize nanomaterial. In this manner, the spectral position and yield of the crystallite fluorescence can be modified by changing the chemical nature of the colloid surface. Hence, it has observed that the higher wavelength peak may come due to some impurity in our material. The presence of defects in the nanoparticle was also supported by the SEM images of the sample (Fig.4).

4. Conclusions

A series of nano crystalline Cr^{+3} -substitution Co-ferrites system ($CoCr_xFe_{2-x}O_4$ where $0.0 \leq x \leq 0.10$ with interval 0.02) synthesized by co-precipitation technique and sintered at 900^{o}C for 6 h. The effect of Cr^{+3}-content on the structural parameters has been studied. X-ray diffraction confirmed that the high degree of order and monodispersity of the nano-particles that exhibits the single phase face center cubic structure (FCC). The physical parameters of the material revealed that the crystallite size were found in the range (31.5-70.4 nm) while lattice parameter, X-ray density decreases with the increase of Cr^{+3}-concentrations. So, the degree of "quantum confinement" in these spinel ferrites was determined from their optical absorption and photoluminescence spectra.

Acknowledgements

Corresponding author (Ghulam Mustafa) is thankful to Dr Akbar Ali for providing the experimental facilities at COMSATS Institute of Information Technology, Lahore, Pakistan.

References

[1] R GKharabe, R SDevan, CM Kamadi,B KChougule, Smart Material Structures. **15**,36(2006).
[2] K. Prasad,A.K. Jha, Natural Science,**1,** 129 (2009).
[3] A.K.Arora, S.Devi, V.S.Jaswal, J.Singh, M. Kinger, V.D. Gupta, Oriental Journal of Chemistry,**30,** 1671 (2014).
[4] J. Zhang, L. Zhang, X. Peng, X. Wang, Appl. Phys.A,**73**,773 (2001) .
[5] S. L. Pan, D. D. Zeng, H. L. Zhang, H. L. Li,Appl. Phys. A, **70**,637 (2000).
[6] S.S. More, R.H. Kadam, A.R. Shite, D.R. Mane, K.M. Jadhav, J. Alloy Compd. **502,**477 (2010).
[7]A.A. Birajdar, S.E. Shirsath, R.H.Kadam, S.M. Patange, D.R. Mane, A.R. Shitre, Ceram. Int. **38**, 2963 (2012).
[8] A.M. Sankpal, S.S. Suryavanshi, S.V.Kakatkar, G.G. Tengshe, R.S. Patil, N.D.Chaudhari, S.R. Sawant, J. Magn. Magn.Mater.**186**, 349 (1998)
[9] A.Lakshman, K.H. Rao, R.G Mendiratta, J. Magn. Magn.Mater.**250**, 92 (2002).
[10]PothapalayamMahaliPonnusamy,SanthanamAgilan, NatarajanuthuKumarasamy, Dhayalan Velauthapillai,MagneticJ. ZeitschriftfürPhysikalischeChemie. **2196-7156**, 0942 (2015)
[11] Prakash Chand, Anurag Gaur, Ashavani Kumar, Inte.J.Chem.Molec.Nucl.Mater.and Metallu.Engine.**8**,12 (2014).
[12]SantoshBhukal, TseringNamgyal, S.Mor, S. Bansal, SonalSinghalJ.Molec.Stru. **1012,**162 (2012).
[13] M. M Bahout, S.Bertrand, O. Pena, J. Solid. State.Chem. **178**, 1080 (2005).
[14] KatalinSinkoEnik,Manek,Aniko,Meiszterics,Ka´rolyHavancsaUlla VainioHerwig Peterlik, J.Nanopart Res (2012)
[15] K.Maaz, ArifMumtaz, S.K. Hasanain, Abdullah Ceylan, J. of Magnetism and Mag. Materials **308,**289 (2007).
[16] A.Pradeep, PriyaDarshini, P, Chandra Sekharan, J. Mater. Chem. Phys. **112**, 572 (2008).
[17] C, Liu, B,Zou, Rondinone, AJ, Zhang, ZJ: Chem. Soc. **122**,6263 (2000).
[18] JLH,Chau, MK, Hsu, CC: Kao, Mater.Lett.**60**,947 (2006).
[19] HM, Deng, J, Ding, Y., Shi, XY,Liu, J. Wang, J. Mater. Sci. **36**, 3273 (2001).
[20] YI.Kim, D.Kim, CS: Lee, Phys B: Condensed Matter **337**,42 (2003).
[21] N. Amin, M. Imran Arshad, M. U. Islam, A. Ali, K. Mahmood,G. Murtaza, M. Ahamad, G. Mustafa; Digest Journal of Nanomaterials and Biostructures **11**(2), 579 (2016).
[22] B.D. Cullity,secondedition,AddisonWesleyPublishing,Co.92 (1978).
[23] Ghulam Mustafa, M.U. Islam, Wenli Zhang, Yasir Jamil, Abdul Waheed Anwar, Mudassar Hussain, Mukhtar Ahmad, J. Alloys Comp, **618**,428 (2015).
[24]MuhamamdNaeemAshiqa, Muhammad Fahad Ehsan, Muhammad Javed Iqbal, Iftikhar Hussain Gul, Journal of Alloys and Compounds **509**,5119 (2011).
[25] A.M.El-Sayed,Ceram.Int.**28**,651 (2002).
[26]V.A. Potakova, W.D. Zverv and V.P. Romanov, Physics Status Solidi (A). **12**, 623(1972).
[27]William E. Lee, W. Mark Rainforth, Ceramic Microstructures: Property Control by Processing, Kluwer Academic Publishers, (1994).
[28]ChandanBorgohain, Kula Kamal Senapati, Debabrata Mishra, Kanak Ch. Sarma, ProdeepPhukan, Nanoscale, **2**,2250 (2010).
[29]N. Orhan, M. C. Baykul, J.Solid- State Electronics**78**, 147 (2012).
[30]P. Chand, A. Gaur, A. Kumar, J. Allo.andCompounds, **539**, 174 (2012).
[31] K. F. Lin, H. M. Cheng, H. C. Hsu, LI. J. Lin, W. F. Hsieh,J.ChemPhysLett **409**, 208 (2005).
[32] O. S. Polezhaeva, N. V. Yaroshinskaya, V. K. Ivanov, Russian Journal of Inorganic Chemistry, **52,**1184 (2007).
[33] D.E. Skinner, D.P. Colombo, J.J. Caveleri, R.M. Bowman, J. Phys. Chem,**99,**7853 (1995).
[34] T.W. Roberti, N.J. Cherepy, J.Z. Zhang, J. Chem. Phys. **108**,2143 (1998).
[35] M.C. Brelle, J.Z. Zhang, J. Chem. Phys. **108**,3119 (1998).
[36] N.J. Cherepy, D.B. Liston, J.A. Lovejoy, H.M. Deng, J.Z. Zhang, J. Phys. Chem.B

102, 770 (1998).
[37]M.C. Brelle, J.Z. Zhang, L. Nguyen, et al J. Phys. Chem. A **103**,10194 (1999).
[38] A. Sengupta, B. Jiang, K.C. Mandal, et al, J. Phys. Chem. B **103**,3128 (1999).
[39] U. Resch, A. Eychmuller, M. Hasse, H.Wellner, Langmuir **8**,2215 (1992).
[40] Y. Lin, J. Zhang, E.H. Sargent, E. Kumacheva, Appl. Phys. Lett. **81**,3134 (2002).
[41] N. Chestoy, T.D. Harris, R. Hull, L.E. Brus, J. Phys. Chem. **90**,3393 (1986).